Zoosymposia 15: 172–191 (2019)
http://www.mapress.com/j/zs/

ISSN 1178-9905 (print edition)
ZOOSYMPOSIA
ISSN 1178-9913 (online edition)

http://dx.doi.org/10.11646/zoosymposia.15.1.19
http://zoobank.org/urn:lsid:zoobank.org:pub:9D39B789-76F2-4577-9A9B-22247A191470

Combined visualization of echinoderm hard and soft parts using contrast-enhanced micro-computed tomography

ALEXANDER ZIEGLER
Institut für Evolutionsbiologie und Ökologie, Rheinische Friedrich-Wilhelms-Universität, An der Immenburg 1, 53121 Bonn, Germany; E-mail: aziegler@evolution.uni-bonn.de

Abstract

Recent studies have shown that micro-computed tomography (μCT) must be considered one of the most suitable techniques for the non-invasive, three-dimensional (3D) visualization of metazoan hard parts. In addition, μCT can also be used to visualize soft part anatomy non-destructively and in 3D. In order to achieve soft tissue contrast using μCT based on X-ray attenuation, fixed specimens must be immersed in staining solutions that include heavy metals such as silver (Ag), molybdenum (Mo), osmium (Os), lead (Pb), or tungsten (W). However, while contrast-enhancement has been successfully applied to specimens pertaining to various higher metazoan taxa, echinoderms have thus far not been analyzed using this approach. In order to demonstrate that this group of marine invertebrates is suitable for contrast-enhanced μCT as well, the present study provides results from an application of this technique to representative species from all five extant higher echinoderm taxa. To achieve soft part contrast, freshly fixed and museum specimens were immersed in an ethanol solution containing phosphotungstic acid and then scanned using a high-resolution desktop μCT system. The acquired datasets show that the combined visualization of echinoderm soft and hard parts can be readily accomplished using contrast-enhanced μCT in all extant echinoderm taxa. The results are compared with μCT data obtained using unstained specimens, with conventional histological sections, and with data previously acquired using magnetic resonance imaging, a technique known to provide excellent soft tissue contrast despite certain limitations. The suitability for 3D visualization and modeling of datasets gathered using contrast-enhanced μCT is illustrated and applications of this novel approach in echinoderm research are discussed.

Key words: Imaging, phenomics, Echinodermata, PTA, morphomics, staining

Introduction

Like other organisms, echinoderms (Deuterostomia: Echinodermata) are *per se* three-dimensional (3D) objects. Although photographic documentation, histological sectioning, and electron microscopy constitute adequate tools to visualize echinoderm hard or soft parts, these techniques predominantly result in two-dimensional (2D) structural information. However, such data are usually not sufficient for modern analytical approaches that aim to capture the entire structural information of a given organism, e.g. phenomics (Gerlai 2002, Houle 2010) or morphomics (Lucocq *et al.* 2014). Conventional 2D imaging techniques thus to some degree constitute an obstacle for the desirable large-scale fusion of data derived from molecular and morphological research (Ziegler *et al.* 2018).

To facilitate digital morphological analyses in zoology, a set of 3D imaging techniques has become available within the last two decades and some have consequently been applied in echinoderm research as well (Ziegler *et al.* 2010a). Among others, these modern imaging techniques include magnetic resonance imaging (MRI), optical projection tomography (OPT), confocal laser scanning microscopy (CLSM), light sheet microscopy (LSM) as well as the different variants of computed tomography (CT), in particular micro-

 Accepted by K. Kanazawa: 31 Jan. 2019; published: 21 Oct. 2019

computed tomography (μCT) and synchrotron-radiation μCT (SRμCT). While each of these modalities has its specific advantages and disadvantages, μCT is currently emerging as one of the main techniques for future structural studies on echinoderms (Ziegler 2012). The principal reason for this is that μCT permits detailed, non-invasive analyses of mineralized structures (Stauber & Müller 2008).

As conventional μCT studies are based on the principle of X-ray attenuation, hard parts will usually be the primary focus of analysis. Following the pioneering study by Stock *et al*. (2002), the capacity of μCT to accurately depict mineralized echinoderm tissues in 3D has so far been demonstrated in studies on extant crinoids (Aschauer *et al*. 2010, Ziegler 2012), asteroids (Ziegler 2012, Ziegler & Menze 2013, Blowes *et al*. 2017, Schwertmann *et al.* 2019), ophiuroids (Ziegler 2012, Landschoff & Griffiths 2015, Okanishi *et al*. 2017, Clark *et al.* 2019), echinoids (Stock *et al*. 2003, 2004a, 2012; Ziegler *et al*. 2010a; Mihaljević *et al*. 2011; Ziegler 2012; Ziegler & Menze 2013; Goetz *et al*. 2014; Grun & Nebelsick 2018a, 2018b; Lauer *et al*. 2018), and holothuroids (Reich 2015) as well as a diverse array of fossil echinoderm taxa (Rahman & Clausen 2009, Zamora *et al*. 2012, Rahman *et al*. 2015, Reid et al. 2018). In addition, several high-resolution SRμCT studies (David *et al.* 2009; Rahman & Zamora 2009; Stock *et al.* 2004b, 2006, 2010, 2013, 2017; Stock & Rack 2014; Ziegler *et al.* 2010b, 2012a; Souto & Martins 2018) as well as two clinical CT studies conducted using larger specimens (Martony *et al.* 2018, Mihaljević & Rosenblatt 2018) have further illustrated the feasibility of X-ray-based 3D imaging on echinoderms. In addition, while the above-mentioned studies have made use of the capacity of CT systems to gather 3D datasets, the same scanners can also be used to obtain conventional 2D X-ray images (Mihaljević *et al.* 2011, Ziegler *et al.* 2016, Ziegler & Barr 2018), effectively expanding the potential range of applications for analyses based on this technology.

The main focus of all previous studies on echinoderms illustrates that CT techniques are primarily suited for research on mineralized structures such as teeth, spines, jaws, tests, or joints. However, echinoderms are obviously not composed of calcified structural elements alone, but also consist of varying amounts of soft tissues that are informative in a number of ways. It would thus be desirable to have access to a technique allowing soft part visualization at high resolution and in 3D, but without the need to alter the structural integrity of a specimen.

In order to visualize metazoan soft tissues digitally, non-invasively, and in 3D only a limited number of techniques can be employed, in particular clinical or preclinical MRI (Boistel *et al.* 2011; Zanette *et al.* 2014; Ziegler *et al.* 2011a, 2018). Apart from research on various other Metazoa, in particular preclinical MRI has in the past successfully been used to obtain soft part information from living as well as fixed echinoderm specimens (Ziegler & Angenstein 2007; Ziegler *et al.* 2007, 2008, 2009, 2010c, d; Sigl *et al.* 2013), but also from a fossil taxon (Mietchen *et al.* 2008). However, preclinical MRI is a complex technology that may not be readily accessible, primarily due to a comparatively low world-wide distribution of the respective systems (Ziegler *et al.* 2008). In addition, MRI has certain limitations with regard to its maximally achievable resolution and can be prone to artifacts, for example at tissue boundaries or when air bubbles and particularly para-or ferromagnetic objects are located within a specimen (Ziegler & Mueller 2011, Ziegler *et al.* 2011a).

To circumvent some of these problems, a powerful addition to MRI is presently emerging in the form of contrast-enhanced μCT. This approach entails the application of various contrast agents to increase the density of soft tissues, thus increasing their capacity for X-ray attenuation and hence their visibility in CT-based studies (Metscher 2009, Gignac *et al.* 2016). As contrast-enhanced μCT has so far been successfully applied to a broad range of metazoan organisms, the aim of the present study was to analyze whether this approach could also be used to study echinoderms. To this end, representative species from all five higher extant echinoderm taxa, i.e. feather stars (Crinoidea), sea stars (Asteroidea), brittle stars (Ophiuroidea), sea urchins (Echinoidea), and sea cucumbers (Holothuroidea) were included in the present analysis. Formalin-fixed, ethanol-preserved specimens were immersed in phosphotungstic acid (PTA), a staining solution containing tungsten (W). This heavy metal had previously been shown to provide good soft part contrast in different invertebrate and vertebrate taxa (Metscher 2009, Ziegler & Menze 2013, Fernández *et al.* 2014, Xavier *et al.* 2015, Herzog *et al.* 2017, Chen *et al.* 2018, Jahn *et al.* 2018, Weinhardt *et al.* 2018, Ziegler *et al.* 2018). The resulting datasets were qualitatively analyzed to evaluate whether a combined visualization of hard and soft parts would entail advantages for morphological and anatomical inferences in echinoderm research.

Materials and Methods

Specimens

Live animals were obtained during low tide from beaches and rocky shores near Concarneau, France. Specimens were identified to species level using keys for echinoderm taxa occurring in the Northeastern Atlantic (Hayward & Ryland 1996). In addition, museum wet specimens from the Department of Invertebrate Zoology, California Academy of Sciences, San Francisco, CA, USA (CASIZ) and the Abteilung Marine Invertebraten, Museum für Naturkunde, Berlin, Germany (ZMB) were used to complement the available sample of living material. All freshly fixed specimens used in the present study have been deposited in the echinoderm wet collection of the ZMB (Tab. 1).

Preparation of specimens

Live animals were relaxed for 2 h using a 7% $MgCl_2$ solution in sea water before transfer to a fixative of 5% formalin in sea water. After one week of storage in this solution, the specimens were rinsed using cold tap water and gradually transferred to 70% ethanol. After another week of storage in ethanol, the freshly fixed as well as the museum specimens were transferred each to a plastic container with 50 ml of 0.3% PTA in 70% ethanol (Metscher 2011). Diffusion-based staining was conducted over a period of four weeks with occasional gentle shaking of the container. Shortly before µCT scanning, the specimens were removed from the staining solution, placed in tight plastic tubes to prevent movement during the scan, and immersed in clean 70% ethanol.

Micro-computed tomography

Analyses using µCT were conducted on seven stained and two unstained specimens (Tab. 1). All nine organisms were scanned with soft parts preserved. The two unstained specimens had previously (Ziegler 2012) been studied using a Phoenix Nanotom system with a detector size of 2,304 × 2,304 px (GE Sensing & Inspection Technologies, Wunstorf, Germany). The seven PTA-stained specimens were scanned using a SkyScan 1272 system with a detector size of 4,032 × 3,280 px (Bruker microCT, Kontich, Belgium). Scanning parameters were adapted to suit the specific needs of each object (Tab. 1). Reconstruction of the 2D projection images into a 3D volume composed of 16-bit image files was accomplished without compression using the software packages DatosX Reconstruction 1.5 (GE Sensing & Inspection Technologies) and NRecon 6.4 (Bruker microCT).

Magnetic resonance imaging

In addition to the acquired µCT scans, previously gathered MRI datasets from three echinoid species, i.e. *Psammechinus miliaris* (P.L.S. Müller, 1771), *Echinocyamus pusillus* (O.F. Müller, 1776), and *Echinocardium cordatum* (Pennant, 1777) were downloaded from the online repository *GigaDB*. Voxel resolution of these three datasets was 44 µm isotropic for *P. miliaris*, 18 × 18 × 20 µm for *E. pusillus*, and 81 µm isotropic for *E. cordatum*. Additional information about each specimen and the specific scanning parameters are provided in the publication accompanying the deposited dataset (Ziegler *et al.* 2014).

Histology

For further comparative purposes, a single adult specimen of *E. pusillus* collected near Heligoland, Germany was fixed in Bouin's solution for 24 h, decalcified in 2% nitric acid, dehydrated in an ethanol series, and embedded in paraffin. A complete series of 8 µm thick sections was prepared using a 2050 Supercut microtome (Reichert-Jung, Nußloch, Germany) and stained using Azan. Images of selected sections were acquired using an MZ16A stereomicroscope with attached digital camera for documentation (Leica Mikrosysteme, Wetzlar, Germany).

Dataset visualization

The hardware used for 2D and 3D dataset visualization included a multi-core processor with random access memory (RAM) of 128 GB and video RAM of 24 GB running on a 64-bit Windows 10 operating system (Microsoft Corp., Redmond, WA, USA). The µCT data were transformed to 8-bit tagged image file format (TIFF) stacks using the free software Fiji (Schindelin *et al.* 2012). Apart from this tool, the commercial software packages Amira 6.7 (Thermo Fisher Scientific, Waltham, MA, USA) and VGSTUDIO MAX 3.3 (Volume Graphics GmbH, Heidelberg, Germany) were used for dataset visualization. Inspection in 2D was

TABLE 1. Systematically arranged list of echinoderm specimens analyzed using µCT, including respective scanning parameters.

	***Antedon bifida* (Pennant, 1777)**	***Asterina gibbosa* (Pennant, 1777)**	***Ophiothrix fragilis* (Abildgaard in O. F. Müller, 1816)**	***Paracentrotus lividus* (Lamarck, 1816)**	***Echinocyamus pusillus* (O. F. Müller, 1776)**	***Echinocyamus pusillus* (O. F. Müller, 1776)**	***Echinocardium cordatum* (Pennant, 1777)**	***Echinocardium cordatum* (Pennant, 1777)**	***Oestergrenia digitata* (Montagu, 1815)**
Taxonomy	Crinoidea: Antedonidae	Asteroidea: Asterinidae	Ophiuroidea: Ophiotrichidae	Echinoidea: Parechinidae	Echinoidea: Echinocyamidae	Echinoidea: Echinocyamidae	Echinoidea: Loveniidae	Echinoidea: Loveniidae	Holothuroidea: Synaptidae
Specimen	ZMB Ech 7434	ZMB Ech 7435	ZMB Ech 7436	ZMB Ech 7437	ZMB Ech 7410	CASIZ 112655	ZMB Ech 7407	ZMB Ech 7439	ZMB Ech 7438
Locality	Concarneau, France	Concarneau, France	Concarneau, France	Concarneau, France	Heligoland, Germany	Firth of Lorn, United Kingdom	Heligoland, Germany	Concarneau, France	Concarneau, France
Scanner	SkyScan 1272	SkyScan 1272	SkyScan 1272	SkyScan 1272	Phoenix Nanotom	SkyScan 1272	Phoenix Nanotom	SkyScan 1272	SkyScan 1272
Contrast agent	0.3% PTA in 70% ethanol	0.3% PTA in 70% ethanol	0.3% PTA in 70% ethanol	0.3% PTA in 70% ethanol	-	0.3% PTA in 70% ethanol	-	0.3% PTA in 70% ethanol	0.3% PTA in 70% ethanol
Detector size	4,032 × 3,280 px	4,032 × 3,280 px	4,032 × 3,280 px	4,032 × 3,280 px	2,304 × 2,304 px	4,032 × 3,280 px	2,304 × 2,304 px	2,452 × 1,640 px	4,032 × 3,280 px
Source voltage	90 kV	100 kV	90 kV	100 kV	90 kV	100 kV	100 kV	90 kV	80 kV
Source current	111 µA	100 µA	111 µA	100 µA	160 µA	100 µA	160 µA	111 µA	125 µA
Isotropic voxel resolution	5 µm	6.5 µm	5 µm	5 µm	9 µm	4 µm	13.91 µm	10.8 µm	5 µm
Exposure	3,714 ms	9,644 ms	3,714 ms	5,171 ms	750 ms	5,171 ms	750 ms	2,805 ms	2,619 ms
Angular steps	0.3° over 180°	0.2° over 180°	0.3° over 180°	0.3° over 180°	0.3° over 360°	0.3° over 180°	0.3° over 360°	0.3° over 180°	0.3° over 180°
Averages	4	4	4	4	2	3	2	5	4
Random movement	15 px	15 px	15 px	15 px	-	-	-	15 px	15 px
Filter	Al 0.5 + Cu 0.038 mm	Cu 0.11 mm	Al 0.5 + Cu 0.038 mm	Cu 0.11 mm	Cu 0.2 mm	Cu 0.11 mm	Cu 0.2 mm	Al 0.5 + Cu 0.038 mm	Al 1 mm
Acquisition time	3 h 57 min 15 s	13 h 29 min 46 s	3 h 56 min 23 s	5 h 15 min 17 s	1 h 18 min 5 s	3 h 9 min 19 s	1 h 15 min 11 s	3 h 23 min 39 s	13 h 45 min 36 s
Figure	3	4	5	6	1A-D	1E-H, 2C	8C	8D	7
Source	This study	This study	This study	This study	Ziegler (2012)	This study	Ziegler (2012)	This study	This study

carried out using the *Volume Viewer* plugin in Fiji or the *Slice* module in Amira. Visualization of the data in 3D was accomplished by volume rendering using the *Phong shading* algorithm in VGSTUDIO MAX or the *Volume Rendering* module in Amira.

Dataset deposition

A Morphobank project (#3268) was created as public repository for digital 2D and 3D data generated in the course of this study (Ziegler 2019). The deposited information includes nine tomographic datasets and 45 media files amounting to a total size of 1.2 GB. In order to provide standardized results and reduce data size, all deposited 3D datasets were binned to 20 µm isotropic voxel resolution using the *Scale* function in Fiji.

Results

As the capacity of µCT to visualize echinoderm hard parts *in situ* at adequate resolutions had previously been demonstrated, the process to replicate these results was straightforward. The first experiment was thus performed using an unstained specimen of the minute sand dollar species *Echinocyamus pusillus* (Fig. 1A–D). The data show that despite this specific sample being scanned with preserved soft parts, only hard parts such as test with spines (Fig. 1A, B) or Aristotle's lantern with pyramids and teeth (Fig. 1C, D) can be seen.

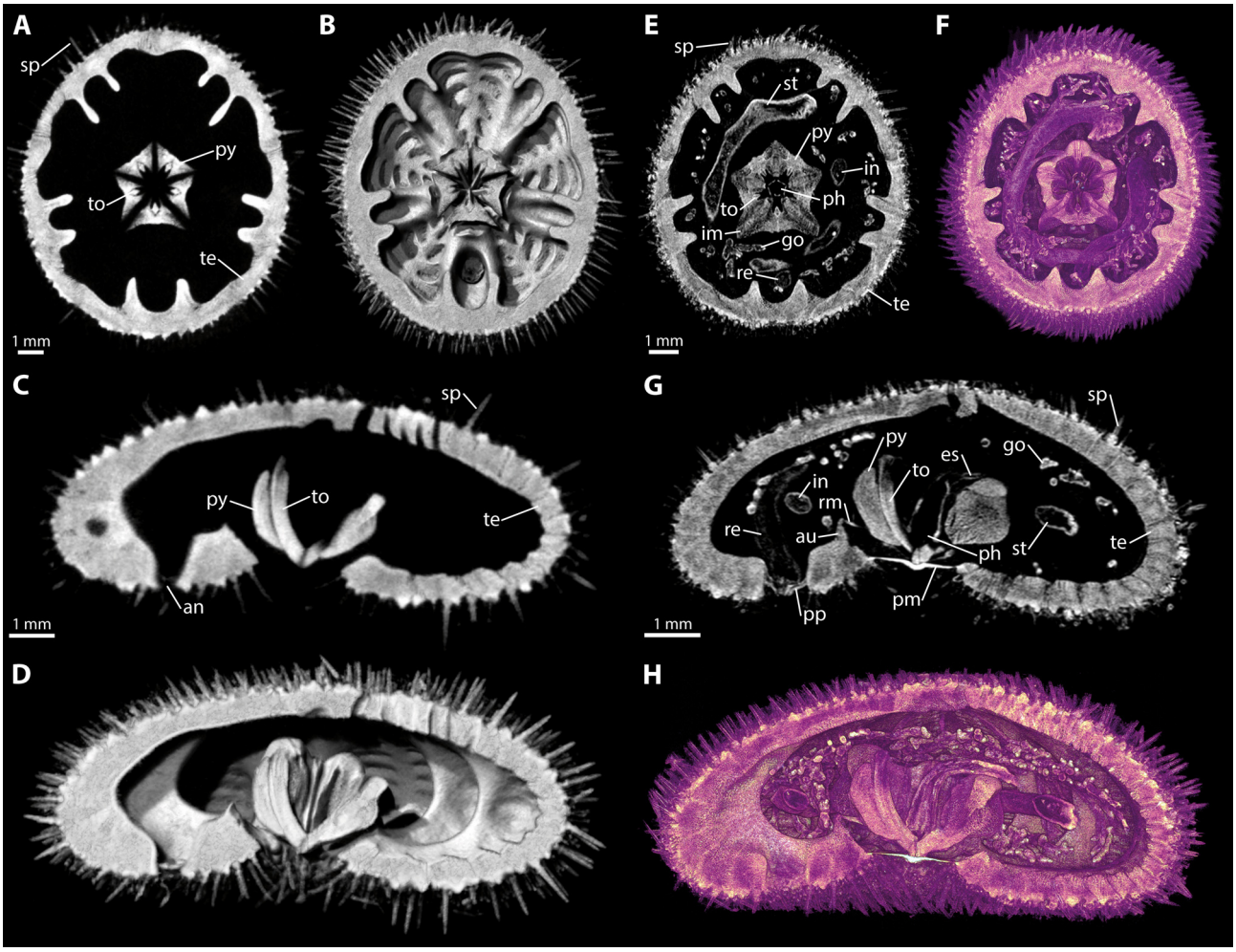

FIGURE 1. Comparison of µCT scans of two differently treated adult specimens of the minute echinoid *Echinocyamus pusillus*, both with soft parts preserved. Specimen ZMB Ech 7410 (A–D) was scanned without application of a contrast agent, while specimen CASIZ 112655 (E–H) was scanned following PTA-staining. (A, E) Virtual transverse section at the mid-level of Aristotle's lantern. (B, F) Virtual transverse slicing of a volume rendering, aboral view. (C, G) Virtual sagittal section at the mid-level of the peristomial membrane. (D, H) Virtual sagittal slicing of a volume rendering, lateral view. an = anus, au = auricle, es = esophagus, go = gonad, im = interpyramidal muscle, in = intestine, pe = peristomial membrane, ph = pharynx, pp = periproctal membrane, py = pyramid, re = rectum, rm = retractor muscle, sp = spine, st = stomach, te = test, to = tooth.

In contrast, µCT data obtained in a second experiment using a PTA-stained specimen of the same species illustrate that the contrast agent significantly increases the capacity of soft tissues for X-ray attenuation (Fig. 1E–H). These data show that in addition to the hard parts that were already visible in the previous scan of an unstained specimen (Fig. 1A–D), this dataset of a stained organism provides information on all major internal structures such as the digestive tract, musculature, and reproductive organs (Fig. 1E, F). In addition, the stain permits visualizing structures composed of mutable collagenous tissue (MCT) such as the peristomial membrane (Fig. 1G, H).

As a third experiment, the µCT data gathered from the stained specimen of *E. pusillus* were compared to data obtained using MRI (Fig. 2A) and histology (Fig. 2B). The contrast-enhanced µCT dataset (Fig. 2C) illustrates a number of advantages and disadvantages of this specific approach. While the main organ systems such as the gonads, digestive tract, nervous system, or lantern musculature can be discerned using all three modalities (Fig. 2A–C), resolution and thus level of detail is highest in case of the light-microscopical image of a histological section (Fig. 2B). However, the inevitable process of decalcification has led to the complete loss of hard part information, while physical alteration during sectioning has additionally resulted in a distortion of the specimen's shape, including ruptures of the body wall (Fig. 2B). In turn, a direct comparison of MRI and µCT data shows that the detailed depiction of hard parts in case of the MRI scan (Fig. 2A) is less pronounced than in the PTA-stained sample (Fig. 2C). Contrast-enhanced µCT thus effectively combines the advantages of µCT hard and MRI soft part imaging. In addition, µCT as used here did achieve approximately five times better isotropic voxel resolution than attainable using MRI in specimens of the same size (i.e., 4 µm vs. 20 µm).

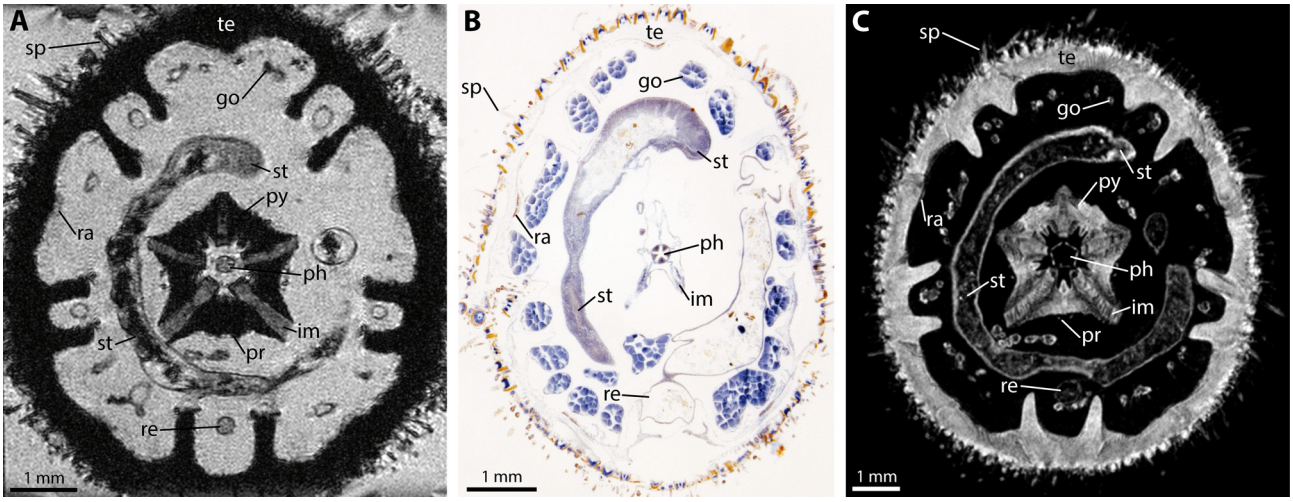

FIGURE 2. Comparison of different techniques used to structurally analyze the minute echinoid *Echinocyamus pusillus*. (A) Virtual transverse section through an MRI dataset at the mid-level of the stomach. (B) Transverse histological section at the mid-level of the stomach. (C) Virtual transverse section through a contrast-enhanced µCT dataset at the mid-level of the stomach, specimen CASIZ 112655. go = gonad, im = interpyramidal muscle, ph = pharynx, pr = protractor muscle, py = pyramid, ra = radial nerve, re = rectum, sp = spine, st = stomach, te = test.

In the next set of experiments, the approach used to analyze the relatively small echinoid *E. pusillus* was expanded to larger specimens selected as representative for each of the five extant higher echinoderm taxa. The µCT data obtained from a stained adult specimen of the feather star *Antedon bifida* illustrate that the chosen contrast agent is capable of penetrating even the relatively dense areas of stereom present in this crinoid. For example, apart from those soft tissues that cover the mineralized endoskeleton (Fig. 3A–C, E), the stain has also penetrated soft parts contained within the calyx such as the various digestive tract elements (Fig. 3D, F). The combined visualization of crinoid hard and soft parts results in a parallel display of structures with usually significantly disparate X-ray attenuation properties such as brachial ossicles and brachial nerves (Fig. 3D). To complement these 2D virtual sections, false-colored volume renderings (Fig. 3A–C, E) based on the grey-scale µCT data (Fig. 3D, F) illustrate the possibilities offered by computer-based 3D visualization.

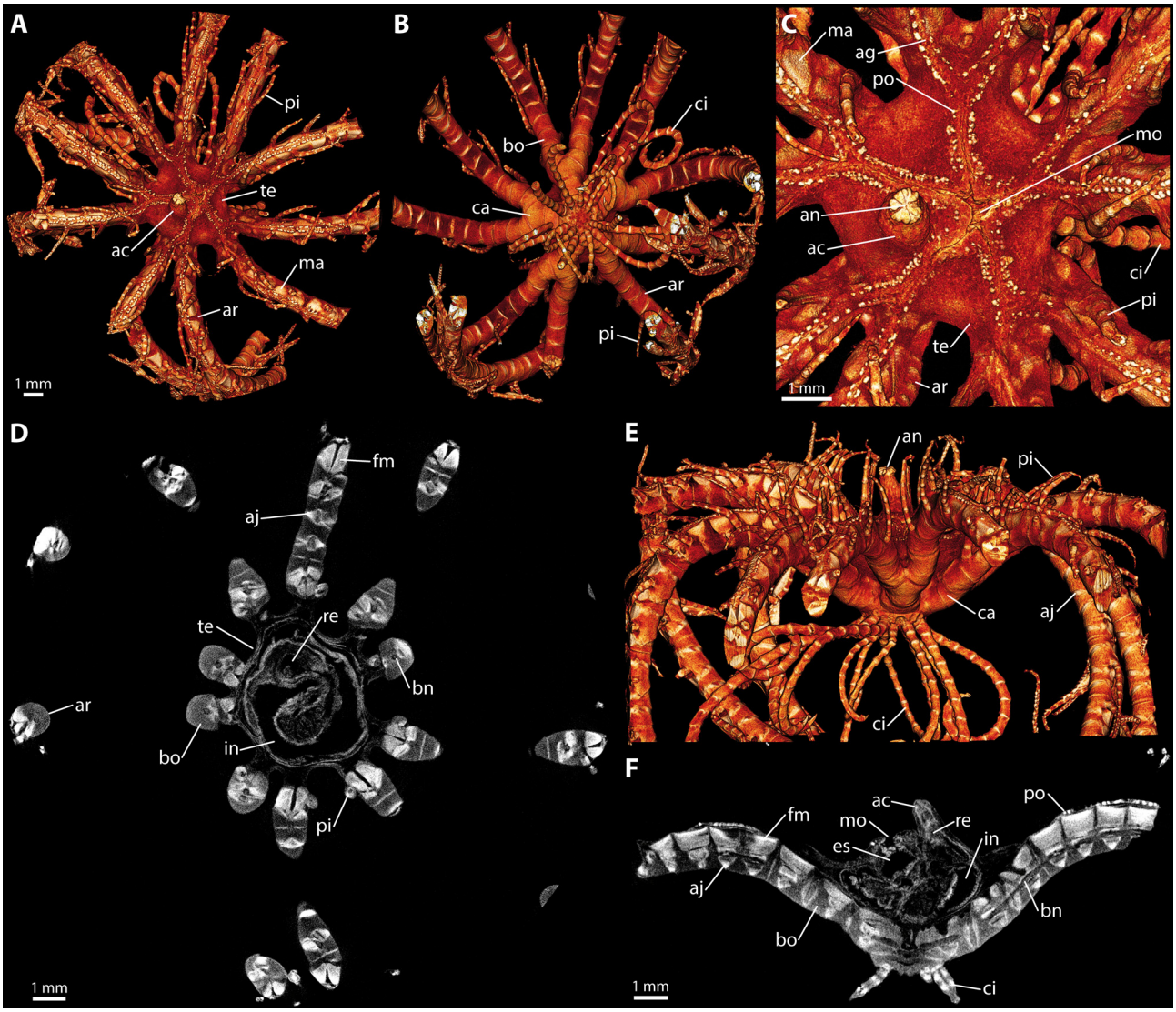

FIGURE 3. Contrast-enhanced µCT of the feather star *Antedon bifida*. The images show results from a scan of PTA-stained specimen ZMB Ech 7434. (A) Volume rendering of the entire dataset, oral view. (B) Volume rendering, aboral view. (C) Close-up of the oral side of the calyx. (D) Virtual transverse section at the level of the intestine. (E) Volume rendering, lateral view. (F) Virtual sagittal section at the level of mouth and anal cone. ac = anal cone, ag = ambulacral groove, aj = arm joint, an = anus, ar = arm, bn = brachial nerve, bo = brachial ossicle, ca = calyx, ci = cirrus, es = esophagus, fm = flexor muscle, in = intestine, ma = marsupium, mo = mouth, pi = pinnule, po = podium, re = rectum, te = tegmen.

The next dataset of a PTA-stained specimen was generated using an adult specimen of the sea star *Asterina gibbosa*. It shows that external hard structures such as spines (Fig. 4A, E), but also soft parts like tube feet, terminal discs, and the partially extruded cardiac stomach (Fig. 4B) can be identified. Using virtual slicing of the volume-rendered 3D data, internal organs such as pyloric caeca, radial nerves, and the pyloric stomach are exposed (Fig. 4C). Virtual sections of the original dataset along two different axes show that all soft tissues have been stained by the contrast agent. Apart from larger organ systems like the pyloric caeca or stomach (Fig. 4D), more minute structures such as the intestine, pyloric ducts, or the ring nerve can be discerned (Fig. 4F).

A PTA-stained adult specimen of the brittle star *Ophiothrix fragilis* was scanned as representative taxon for ophiuroids. As in the case of the crinoid specimen, the anatomically and morphologically largely redundant arms were not scanned in their entire length in order to profit from the higher voxel resolution that a smaller field of view (FOV) entails. Aboral, oral, and lateral views of volume renderings of this dataset illustrate the capacity of contrast-enhanced µCT to visualize ophiuroid hard parts such as the central plate, radial shields, and spines (Fig. 5A) as well as ventral arm plates and bursal slits (Fig. 5B). In addition, external

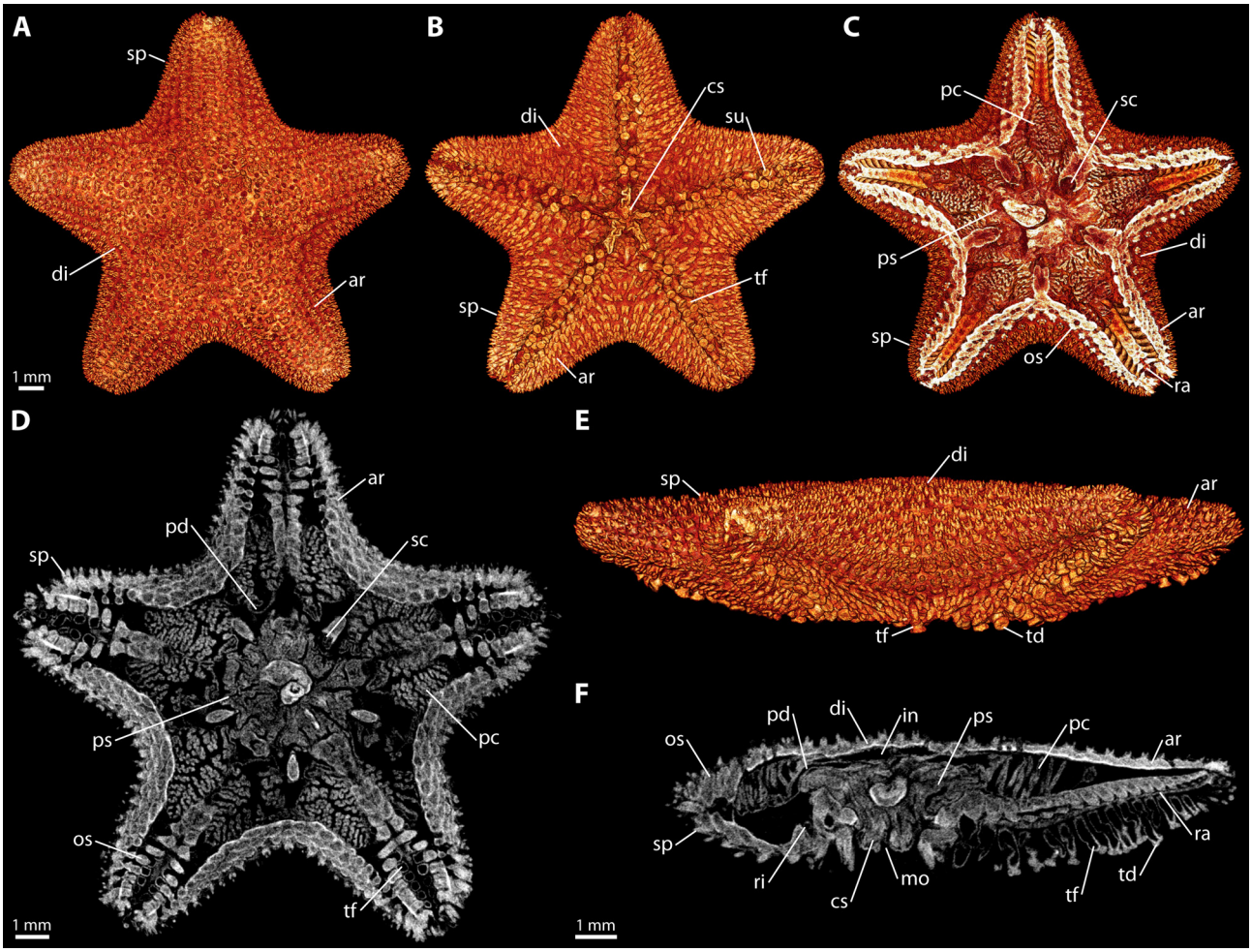

FIGURE 4. Contrast-enhanced µCT of the sea star *Asterina gibbosa*. The images show results from a scan of PTA-stained specimen ZMB Ech 7435. (A) Volume rendering of the entire dataset, aboral view. (B) Volume rendering, oral view. (C) Virtual transverse slicing of a volume rendering at the level of the pyloric stomach, aboral view. (D) Virtual transverse section at the level of the pyloric caeca. (E) Volume rendering, lateral view. (F) Virtual sagittal section at the mid-level of the mouth. ar = arm, cs = cardiac stomach, di = disc, in = intestine, mo = mouth, os = ossicle, pc = pyloric caecum, pd = pyloric duct, ps = pyloric stomach, ra = radial nerve, ri = ring nerve, sc = stone canal, sp = spine, td = terminal disc, tf = tube foot.

soft parts like the regular or the buccal tube feet can be readily identified (Fig. 5E). Apart from external structures, the staining agent has also diffused into disc and arms, resulting in visualization of internal organs such as gonads and stomach (Fig. 5C, D) or the interradial muscle, ring nerve, and intervertebral muscle (Fig. 5F).

Analogous to the results obtained initially using the irregular sea urchin *E. pusillus* (Figs. 1E–H, 2C), heavy metal staining of a juvenile specimen of the "regular" echinoid species *Paracentrotus lividus* resulted in successful penetration of external as well as internal soft tissues. Apart from externally visible structures such as spines, tube feet with terminal discs or periproct as well as peristome (Fig. 6A, B, E), internal organs like components of the digestive tract or soft tissues of Aristotle's lantern can be readily discerned (Fig. 6C). In addition, the dataset permits differentiation of structures largely composed of MCT, for example the compass depressors (Fig. 6D) or the peristomial membrane (Fig. 6F). However, particularly thin structures such as tube feet ampullae and haemal vessels cannot be discerned in the present dataset due to its relatively low signal-to-noise ratio (SNR), which is a consequence of the relatively rapid scan protocols used in the course of this this study (Tab. 1).

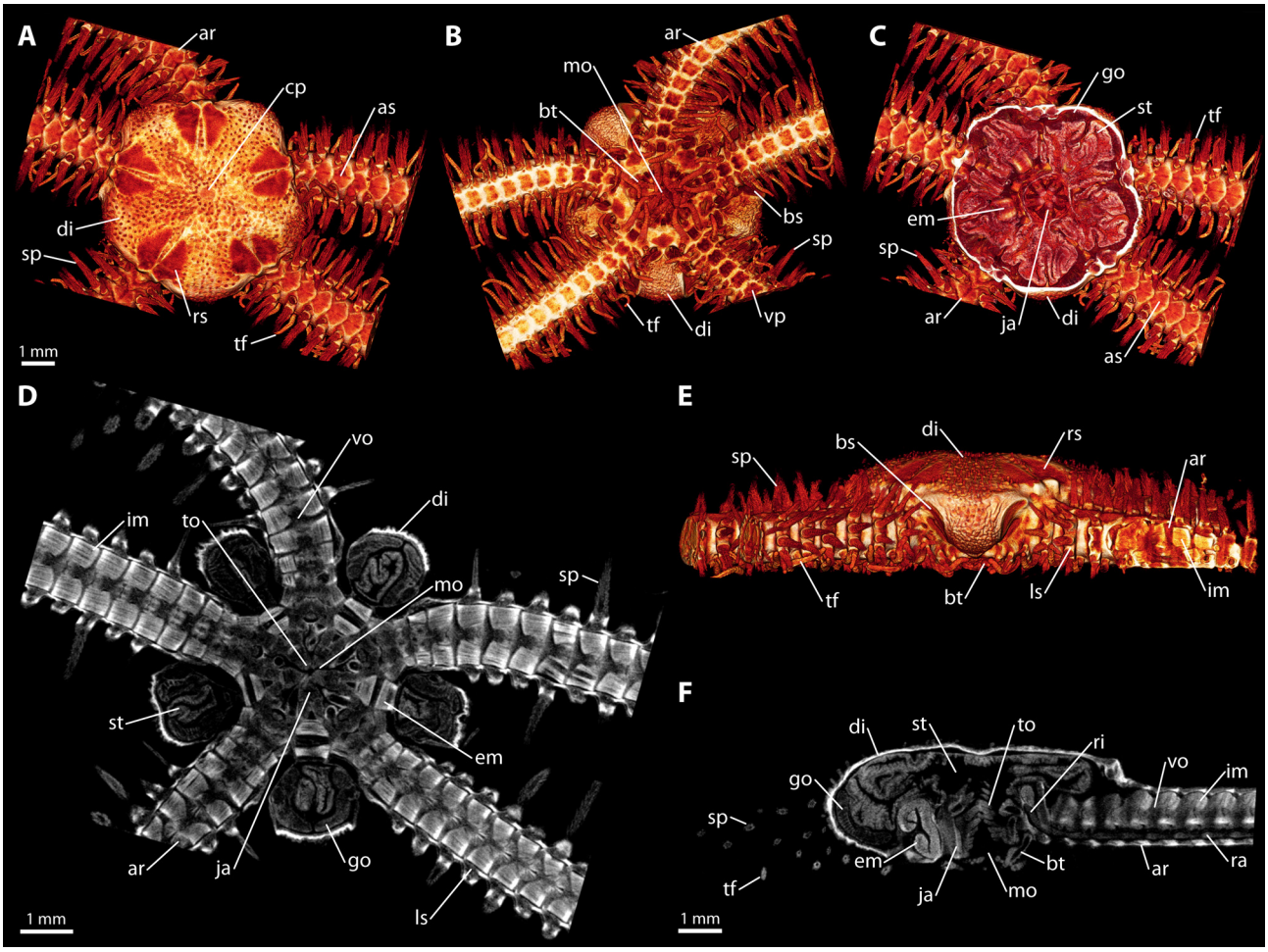

FIGURE 5. Contrast-enhanced µCT of the brittle star *Ophiothrix fragilis*. The images show results from a scan of PTA-stained specimen ZMB Ech 7436. (A) Volume rendering of the entire dataset, aboral view. (B) Volume rendering, oral view. (C) Virtual transverse slicing of a volume rendering at the level of the jaws, aboral view. (D) Virtual transverse section at the level of the gonads. (E) Volume rendering, lateral view. (F) Virtual sagittal section at the mid-level of the mouth. ar = arm, as = arm shield, bs = bursal slit, bt = buccal tube foot, cp = central plate, di = disc, em = external interradial muscle, go = gonad, im = intervertebral muscle, ja = jaw, ls = lateral shield, mo = mouth, ra = radial nerve, ri = ring nerve, rs = radial shield, sp = spine, st = stomach, tf = tube foot, to = tooth, vo = vertebral ossicle, vp = ventral arm plate.

The—from a morphological perspective—most derived echinoderm taxon, the Holothuroidea is here represented by an adult specimen of the sea cucumber *Oestergrenia digitata*. While in all previously scanned echinoderm taxa the relation of hard to soft parts was more or less equal or dominated by hard parts, soft tissues are dominant in sea cucumbers. The volume renderings of aboral, oral, and lateral views show that the contrast agent has diffused into the outer areas of the body wall as well as tentacles (Fig. 7A, B, E). Virtual slicing of a volume-rendered view reveals that the entire body wall has been stained and, with regard to its X-ray attenuation properties is similar to the single large calcareous structure present in most sea cucumbers, the calcareous ring (Fig. 7C). A transverse virtual section of the µCT dataset shows that even more delicate internal organs such as the gonoducts or the dorsoventral mesentery can be visualized successfully (Fig. 7D). Virtual sectioning along the sagittal plane reveals further soft tissue structures such as the rectum, intestine, stomach, esophagus, but also circular and longitudinal muscles as well as epithelium (Fig. 7F). In particular, the complex anatomy of the holothuroid buccal area with tentacle crown, pharynx, ring nerve, retractor musculature, water ring, and further structures can be visualized using contrast-enhanced µCT. However, the body wall ossicles of this particular species are too small to be discernable at the given resolution.

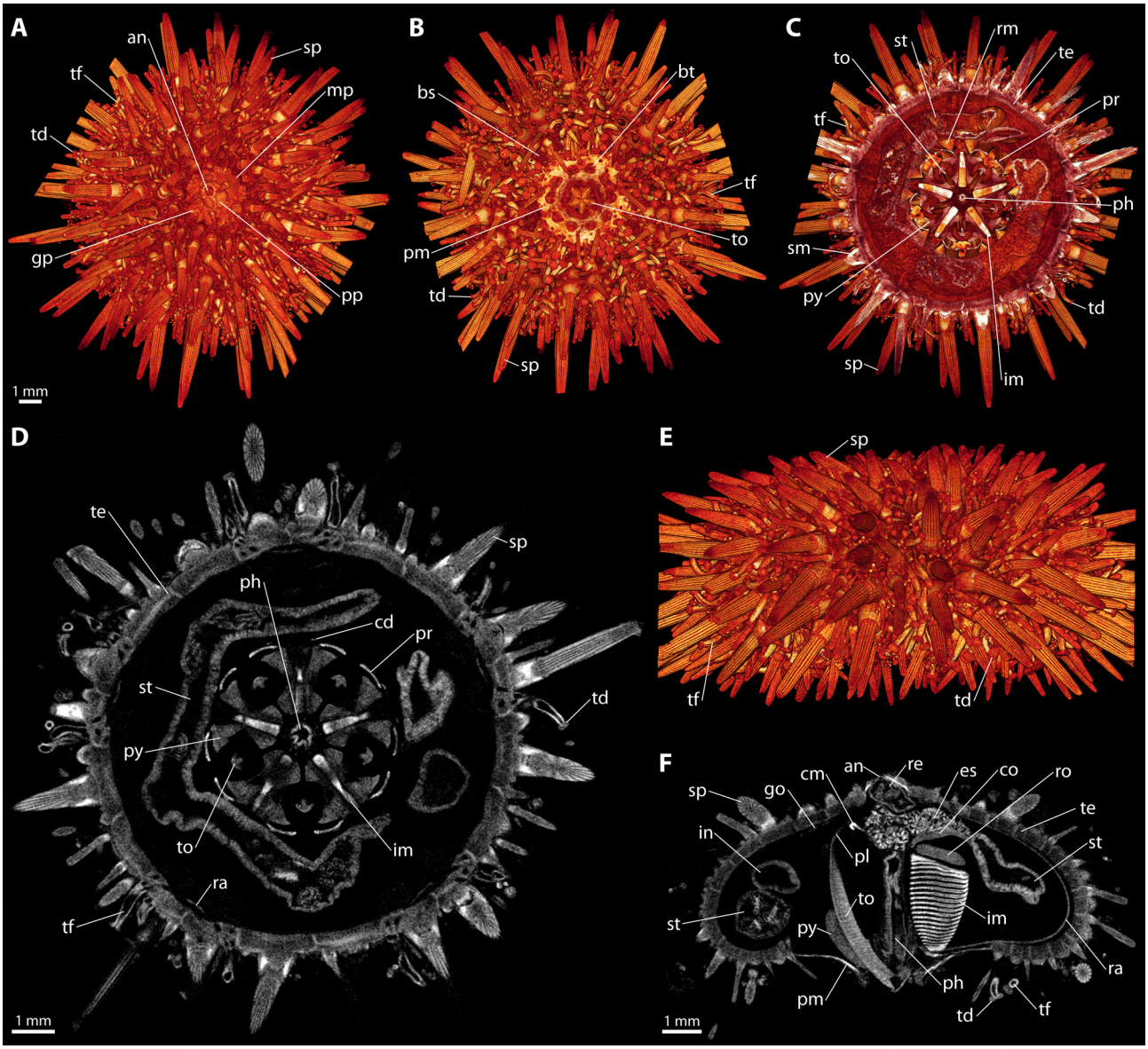

FIGURE 6. Contrast-enhanced µCT of the sea urchin *Paracentrotus lividus*. The images show results from a scan of PTA-stained specimen ZMB Ech 7437. (A) Volume rendering of the entire dataset, aboral view. (B) Volume rendering, oral view. (C) Virtual transverse slicing of a volume rendering at the mid-level of Aristotle`s lantern, aboral view. (D) Virtual transverse section at the level of the stomach. (E) Volume rendering, lateral view. (F) Virtual sagittal section at the mid-level of the pharynx. an = anus, bs = buccal sac, bt = buccal tube foot, cd = compass depressor, co = compass, cm = compass elevator muscle, es = esophagus, go = gonad, gp = genital plate, im = interpyramidal muscle, in = intestine, ph = pharynx, pm = peristomial membrane, pp = periproctal plate, pr = protractor muscle, py = pyramid, ra = radial nerve, re = rectum, rm = retractor muscle, ro = rotula, sm = spine muscle, sp = spine, st = stomach, td = terminal disc, te = test, tf = tube foot, to = tooth.

Finally, a last experiment was conducted to analyze whether contrast-enhanced µCT might be suitable to circumvent specific difficulties encountered during MRI of sediment-feeding echinoderms, in particular certain holothurioid and echinoid taxa. The scan of the bulk-feeding "regular" sea urchin *Psammechinus miliaris* illustrates that MRI in principle provides excellent soft part contrast, even allowing differentiation of minute echinoid gut structures such as the primary siphon (Fig. 8A). However, an MRI scan of a similarly-sized specimen of the sediment-feeding echinoid *Echinocardium cordatum* conducted using scanning parameters largely comparable to those used for *P. miliaris* shows strong artifacts that effectively prohibit the precise recognition of internal organs (Fig. 8B). The primary source of these artifacts, i.e. ingested sediment with para-or ferromagnetic properties can be inferred by analyzing µCT data obtained using an unstained specimen of the same species (Fig. 8C). However, as demonstrated in the first experiment of this study, µCT

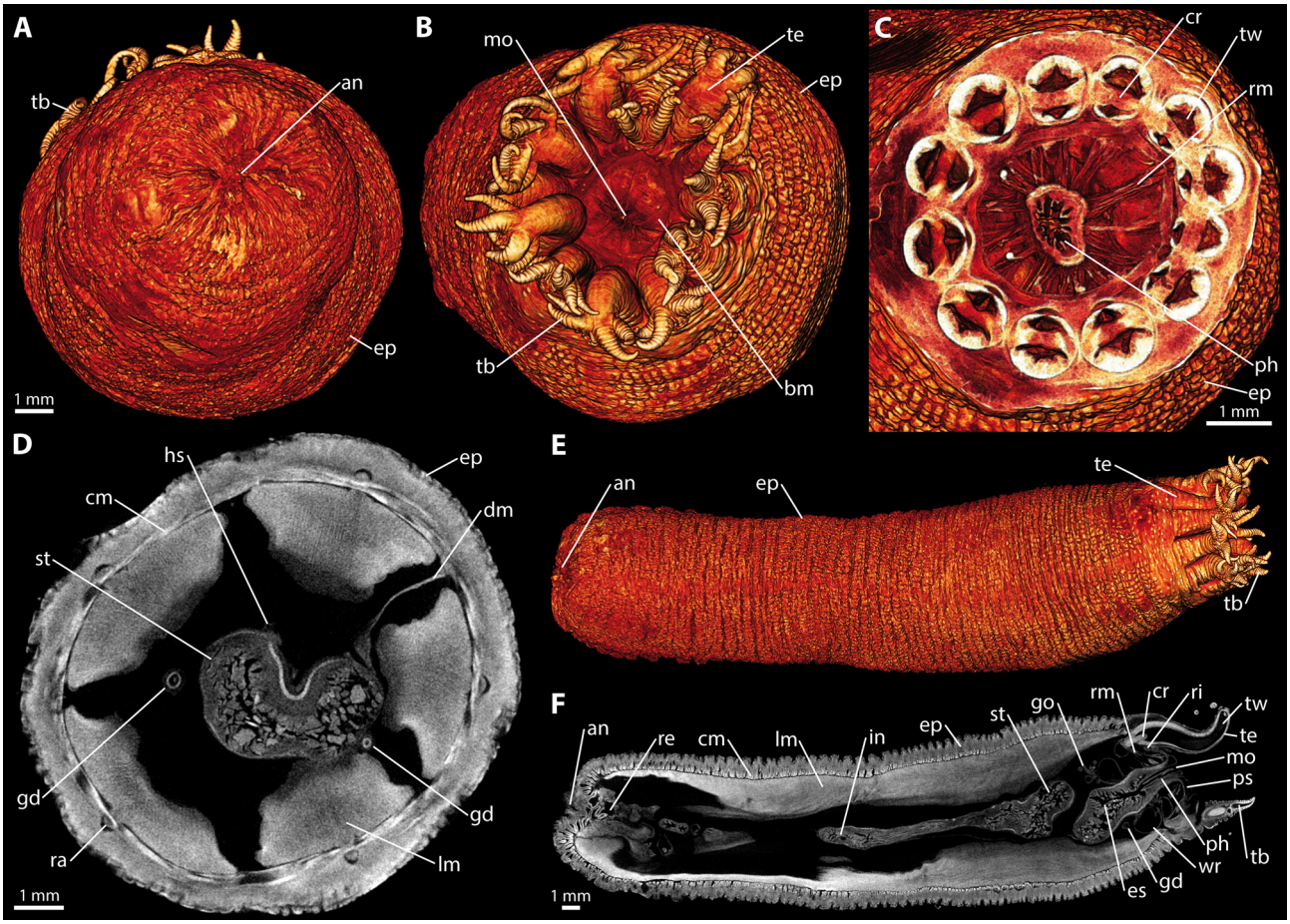

FIGURE 7. Contrast-enhanced µCT of the sea cucumber *Oestergrenia digitata*. The images show results from a scan of PTA-stained specimen ZMB Ech 7438. (A) Volume rendering of the entire dataset, aboral view. (B) Volume rendering, oral view. (C) Virtual transverse slicing of a volume rendering at the level of the calcareous ring, oral view. (D) Virtual transverse section at the level of the stomach. (E) Volume rendering, lateral view. (F) Virtual sagittal section at the mid-level of the intestine. an = anus, bm = buccal membrane, cm = circular muscle, cr = calcareous ring, dm = dorsoventral mesentery, ep = epidermis, es = esophagus, gd = gonoduct, go = gonad, hs = haemal sinus, in = intestine, lm = longitudinal muscle, mo = mouth, ph = pharynx, ps = peribuccal sinus, ra = radial nerve, ri = ring nerve, re = rectum, rm = retractor muscle, st = stomach, tb = tentacular branch, te = tentacle, tw = tentacular water canal.

scanning of unstained specimens usually does not yield any soft tissue information (Fig. 1A–D). In contrast, µCT scanning conducted following specimen staining with PTA permits an artifact-free visualization of hard and soft parts within a single dataset even in the presence of different forms of ingesta (Fig. 8D). With regard to its level of detail, the resulting dataset is comparable to artifact-free MRI data, as illustrated by the visibility of the relatively small primary siphon in these two datasets (Fig. 8A, D).

Discussion

The results obtained in the course of this study show that contrast-enhanced µCT experiments are capable of visualizing soft as well as hard part structures at high isotropic voxel resolutions in echinoderms as well. Contrast-enhanced µCT at present thus must be considered the most suitable tool for a combined, non-destructive 3D visualization of echinoderm hard and soft parts.

Methodological considerations

The staining solution used here, i.e. 0.3% PTA in 70% ethanol provides excellent contrast for a wide range of organ systems. While the capacity of other heavy metal-based staining agents commonly used in contrast-enhanced µCT (Metscher 2009, Fernández *et al.* 2014, Gignac *et al.* 2016) to stain echinoderm tissues was not

evaluated in this study, the main advantage of PTA staining, in particular in comparison with iodine-based agents is that overstaining was not observed, neither in previous (Metscher 2011, Fernández *et al.* 2014, Ziegler *et al.* 2018) nor in the present study. Another advantage of PTA at the given concentration is the absence of tissue shrinkage, an artifact known to occur when iodine-based staining agents are used (Buytaert *et al.* 2014, Gignac & Kley 2014, Gignac *et al.* 2016, Hedrick *et al.* 2018). Furthermore, once prepared, PTA solutions can be stored for extended periods of time (Metscher 2009) and have also been shown to be stable in stained tissues (Lin *et al.* 2018). Finally, as demonstrated here as well as in previous studies (Fernández *et al.* 2014, Ziegler *et al.* 2018), PTA can be used to successfully stain even decades-old museum wet specimens.

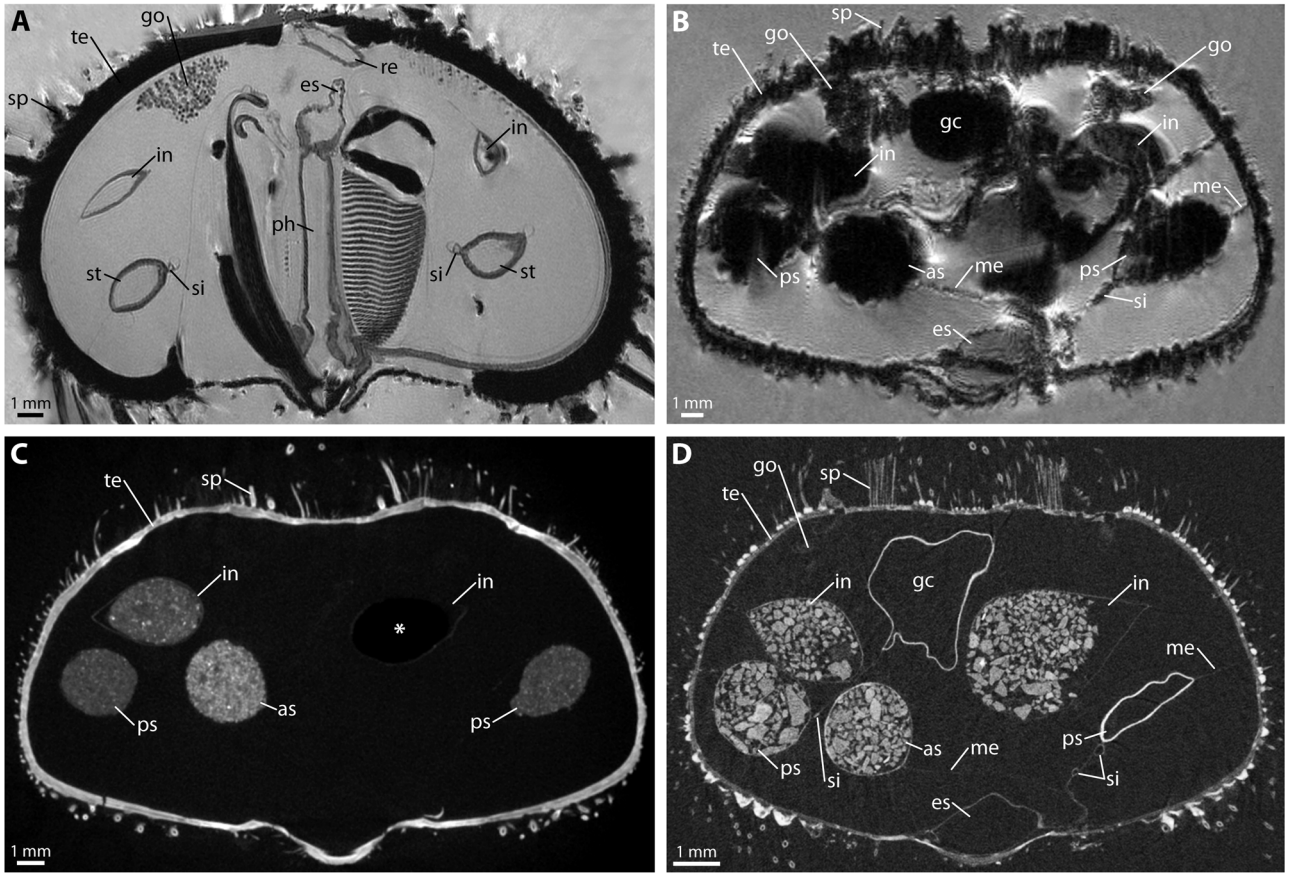

FIGURE 8. Comparison of results derived from MRI and µCT scans of bulk and sediment feeders. (A) Virtual sagittal section through an MRI dataset of the bulk-feeding echinoid *Psammechinus miliaris*. (B) Virtual horizontal section through an MRI dataset of the sediment-feeding echinoid *Echinocardium cordatum*. Note the pronounced artifacts in the vicinity of the digestive tract. (C) Virtual horizontal section through a µCT dataset of *E. cordatum*, unstained specimen ZMB Ech 7407. Asterisk denotes air bubble trapped inside the intestine. (D) Virtual horizontal section through a µCT dataset of *E. cordatum*, PTA-stained specimen ZMB Ech 7439.

However, like is the case with all other currently known staining agents used in contrast-enhanced µCT, tissue contrast following PTA-staining is largely unspecific. This constitutes a significant disadvantage compared to classical histological methods, where chemical agents such as Azan or Mallory's trichrome provide very specific contrast, thus enabling an unequivocal tissue differentiation. However, this deficiency can partially be circumvented by applying multi-channel µCT imaging, an approach that involves sequential scanning of stained specimens using different X-ray energies, thus facilitating tissue differentiation *in silico* (Handschuh *et al.* 2017). This technique might be of particular interest in cases where indiscriminate staining of soft parts in combination with hard parts (e.g. holothurioid tentacles and calcareous ring) will result in a dataset with a relatively complex set of information (Fig. 7C). In addition, the registration or fusion of µCT datasets gathered prior to and following staining could also be taken into consideration in such a scenario (Ziegler *et al.* 2018).

Evidently, the staining of wet specimens with heavy metal-based agents results in an alteration of the sample, which usually will prevent use of type or otherwise rare and valuable material. However, techniques

are likely to become available in the future that will help to remove contrast agents from stained specimens (Schmidbaur *et al.* 2015, Gignac *et al.* 2016). Furthermore, in case of specimens intended for DNA extraction, alterations of the genetic code due to the X-ray dose a sample might receive during scanning cannot be ruled out (Paredes *et al.* 2012, Hall *et al.* 2015, Immel *et al.* 2016, Wanek & Rühli 2016).

One of the principle advantages of µCT in comparison to MRI is the possibility to achieve higher isotropic voxel resolutions in specimens of equal size. In the present study, the geometric resolution achieved for most specimens analyzed using the SkyScan system was close to resolving stereom microstructure, i.e. around 5 µm (Tab. 1). As the focus of the present study was not to visualize this particular mineralized tissue, scan parameters were chosen to realize adequate visualization of the entire specimen, which was accomplished by choosing a larger FOV with in turn lower overall resolution. However, like other µCT scanners of the latest generation, the system used here is capable of delivering isotropic voxel resolutions at the three-digit nanometer scale, thereby approaching conventional light microscopy (Ziegler *et al.* 2018). Obviously, this technical possibility will open up considerable opportunities for research on isolated echinoderm ossicles, but certainly for soft tissue studies as well. Of further interest to echinoderm research could be advances made in the field of µCT-and SR-µCT-based phase contrast imaging, an approach capable of combined soft and hard part visualization without the application of a contrast agent (Zehbe *et al.* 2010, 2012).

Apart from resolution, SNR is an important factor for the visualization of morphological and anatomical structures. To achieve best results with regard to SNR, ideally dry echinoderm specimens are scanned in air, thus making use of the relatively strong contrast between mineralized tissues and air. While heavy metal-stained soft parts should theoretically provide strong contrast as well, wet specimens need to be kept in ethanol during the scan to prevent desiccation and thus potential movement artifacts. However, ethanol and other liquids have significantly higher X-ray attenuation properties than air; therefore, to obtain a similarly good SNR as in case of dry specimens scanned in air, the exposure or alternatively the number of averages used during the scan need to be increased. However, such changes will result in longer acquisition times, which may increase the risk for artifacts due to sagging of the specimen or expansion caused by thermal drift. Therefore, in case of the PTA-stained specimens analyzed here a compromise between SNR and acquisition time was made (Tab. 1), resulting in difficulties to visualize delicate internal organs with sufficient quality (Fig. 6D). To achieve a significantly better SNR, the number of averages would probably have to be increased by a factor of two. Another approach to improve SNR is to treat specimens with critical point drying (CPD) prior to scanning (Aschauer *et al.* 2010). Using this method, wet tissues of a given specimen will be rapidly dried and the sample can then be scanned in air without fear of desiccation and corresponding movement artifacts. A further augmentation of this approach can be achieved by heavy metal-staining of soft tissues prior to CPD (Sombke *et al.* 2015). However, this method obviously constitutes a more invasive approach usually unsuitable for valuable material such as type specimens.

Morphological and anatomical aspects

The datasets presented here illustrate the potential of contrast-enhanced µCT to visualize morphological and anatomical features of a single organism in 3D and in their full, unaltered organismic context. Such data were simply not available before using (semi-)invasive techniques such as dissection, histology, or electron microscopy. However, combined hard and soft tissue visualization provides the researcher with a considerable, if not overwhelming amount of structural information. The correct interpretation of organ systems thus requires a profound understanding of echinoderm anatomy and morphology in order to prevent misidentification of internal or external structures. An example from previous research conducted using echinoids and MRI illustrates the potential for erroneous interpretations of soft tissue structures (Holland & Ghiselin 2009, Ziegler & Bartolomaeus 2009). Therefore, in a scenario where designation of internal organ systems is problematic due to the largely unspecific soft tissue staining obtainable with contrast-enhanced µCT, a correlative approach involving different complementary imaging techniques should be taken into consideration (Handschuh *et al.* 2013).

Despite such impediments, the new possibilities offered by contrast-enhanced µCT constitute a remedy for the fact that echinoderm internal anatomy is—compared to hard-part morphology—a largely overlooked aspect in taxonomic and comparative systematic echinoderm studies. Certainly, of importance in this regard is the potential of contrast-enhanced µCT to generate valuable structural data rapidly, with considerable ease, and at low cost—features that will facilitate large-scale sampling efforts, which form the basis of comparative

anatomical and morphological studies. Within this framework, 3D imaging techniques such as MRI or CT must be seen as valuable extensions of the methodological spectrum allowing novel insights into echinoderm hard and soft part structures that previously would not have been possible using conventional techniques (Ziegler *et al.* 2012b).

Application in echinoderm taxonomy and systematics

Apart from anatomical and morphological studies intended for comparative purposes or functional inferences, contrast-enhanced μCT is now increasingly being used to obtain alpha-taxonomical data. This possibility has so far been used to replace existing, invasive techniques or was carried out to complement data derived from more conventional modalities. Using contrast-enhanced μCT, new species have been described in a number of metazoan taxa, including Myriapoda (Akkari *et al.* 2015), Hirudinea (Tessler *et al.* 2016), Gastropoda (Jochum *et al.* 2017), Hymenoptera (Garcia *et al.* 2017), Bivalvia (Machado *et al.* 2018), and Cnidaria (Gusmão *et al.* 2018). Although specific CT techniques have recently also been used in echinoderm taxonomy (Mihaljević & Rosenblatt 2018, Souto & Martins 2018), these studies focused on echinoderm hard part structures only. But, as the present study illustrates, it is now possible to integrate soft part data into taxonomic or systematic inferences with considerable ease.

Digital morphology in echinoderm research

CT and other non-invasive imaging techniques are characterized by the inherently digital nature of the resulting datasets. This important feature provides the research community with a number of methodological advances that were not available in case of the previously gathered predominantly analog type of data (Ziegler *et al.* 2010a). Specific advantages of studies conducted using digital morphology include the capacity for 3D modeling and visualization (Ziegler *et al.* 2008, 2011b) as well as parallel virtual dissection in real-time (Ziegler & Menze 2013). Several examples from previous studies conducted using echinoids show that in particular the possibility to rapidly inspect 3D datasets from any given perspective can trigger discoveries that would otherwise not have been possible (Ziegler 2014; Ziegler *et al.* 2009, 2010d, 2012b, 2016). Furthermore, studies based on digital morphology may result in data suitable for pattern recognition and shape analysis protocols (Ziegler *et al.* 2012a, Ziegler & Menze 2013), finite element analysis (Herzog *et al.* 2017), or a more interactive communication of complex biological structures (Ziegler *et al.* 2011b). With regard to the letter aspect, digital morphological and anatomical data were shown to enhance academic teaching, for example through 3D interactive virtual as well as additively manufactured physical 3D models (Ziegler & Menze 2013, Kato *et al.* 2016).

However, with regard to the desirable large-scale correlation of data on the geno- and phenotype, presumably one of the most important advantages of digital morphology is the possibility for data deposition in online repositories (Ziegler *et al.* 2010a, Rowe & Frank 2011, Lenihan *et al.* 2014). In case of previous, MRI-based research on sea urchins, 3D datasets made available online resulted in a significant increase in data transparency and opened up the possibility for data mining by third parties (Ziegler *et al.* 2014). An important prerequisite for this approach is enforced data deposition, which constitutes one of the main reasons for the staggering success of the various molecular disciplines. As previously pointed out, enforced data deposition in parallel to the publication of scientific articles should finally become common practice in echinoderm phenomics and morphomics research as well (Ziegler *et al.* 2010a).

Acknowledgements

I would like to express my gratitude to Nina Furchheim for help during specimen collection. Carsten Lüter and Rich Mooi are thanked for providing museum specimens. Furthermore, I am indebted to Cornelius Faber and Felix Beckmann for access to scanning systems. I would also like to thank Andreas Kroh and one anonymous reviewer for their extensive comments that helped to improve the manuscript. Funding for this study was provided by the Deutsche Forschungsgemeinschaft (INST 217/849-1 FUGG).

References

Akkari, N., Enghoff, H. & Metscher, B.D. (2015) A new dimension in documenting new species: high-detail imaging for myriapod taxonomy and first 3D cybertype of a new millipede species (Diplopoda, Julida, Julidae). *PLoS ONE*, 10, e0135243.
https://doi.org/10.1371/journal.pone.0135243

Aschauer, B., Heinzeller, T. & Weinert, P. (2010) Almost within grasp: crinoid organs rendered 3-dimensionally. *In*: Harris, L.G., Böttger, S.A., Walker, C.W. & Lesser, M.P. (Eds.), *Echinoderms: Durham. Proceedings of the 12th International Echinoderm Conference, Durham, New Hampshire, USA, 7-11 August 2006*. A.A. Balkema, Leiden/London/New York/ Philadelphia/Singapore, pp. 9–14.
https://doi.org/10.1201/9780203869543-c2

Blowes, L.M., Egertová, M., Liu, Y., Davis, G.R., Terrill, N.J., Gupta, H.S. & Elphick, M.R. (2017) Body wall structure in the starfish *Asterias rubens*. *Journal of Anatomy*, 231, 325–341.
https://doi.org/10.1111/joa.12646

Boistel, R., Swoger, J., Kržič, U., Fernandez, V., Gillet, B. & Reynaud, E.G. (2011) The future of three-dimensional microscopic imaging in marine biology. *Marine Ecology*, 32, 438–452.
https://doi.org/10.1111/j.1439-0485.2011.00442.x

Buytaert, J., Goyens, J., De Greef, D., Aerts, P. & Dirckx, J. (2014) Volume shrinkage of bone, brain and muscle tissue in sample preparation for micro-CT and light sheet fluorescence microscopy (LSFM). *Microscopy and Microanalysis*, 20, 1208–1217.
https://doi.org/10.1017/S1431927614001329

Chen, K.C., Arad, A., Song, Z.M. & Croaker, D. (2018) High-definition neural visualization of rodent brain using micro-CT scanning and non-local-means processing. *BMC Medical Imaging*, 18, 38.
https://doi.org/10.1186/s12880-018-0280-6

Clark, E.G., Hutchinson, J.R., Darroch, S.A.F., Koch, N.M., Brady, T.R., Smith, S.A. & Briggs, D.E.G. (2018) Integrating morphology and *in vivo* skeletal mobility with digital models to infer function in brittle star arms. *Journal of Anatomy*, 233, 696–714.
https://doi.org/10.1111/joa.12887

David, B., Stock, S.R., De Carlo, F., Hétérier, V. & De Ridder, C. (2009) Microstructures of Antarctic cidaroid spines: diversity of shapes and ectosymbiont attachments. *Marine Biology*, 156, 1559–1572.
https://doi.org/10.1007/s00227-009-1192-3

Fernández, R., Kvist, S., Lenihan, J., Giribet, G. & Ziegler, A. (2014) *Sine systemate chaos?* A versatile tool for earthworm taxonomy: non-destructive imaging of freshly fixed and museum specimens using micro-computed tomography. *PLoS ONE*, 9, e96617.
https://doi.org/10.1371/journal.pone.0096617

Garcia, F.H., Fischer, G., Liu, C., Audisio, T.L., Alpert, G.D., Fisher, B.L. & Economo, E.P. (2017) X-ray microtomography for ant taxonomy: an exploration and case study with two new *Terataner* (Hymenoptera, Formicidae, Myrmicinae) species from Madagascar. *PLoS ONE*, 12, e0172641.
https://doi.org/10.1371/journal.pone.0172641

Gerlai, R. (2002) Phenomics: fiction or the future? *Trends in Neuroscience,* 25, 506–509.
https://doi.org/10.1016/S0166-2236(02)02250-6

Gignac, P.M. & Kley, N.J. (2014) Iodine-enhanced micro-CT imaging: methodological refinements for the study of the soft-tissue anatomy of post-embryonic vertebrates. *Journal of Experimental Zoology B*, 322, 166–176.
https://doi.org/10.1002/jez.b.22561

Gignac, P.M., Kley, N.J., Clarke, J.A., Colbert, M.W., Morhardt, A.C., Cerio, D., Cost, I.N., Cox, P.G., Daza, J.D., Early, C.M., Echols, M.S., Henkelman, R.M., Herdina, A.N., Holliday, C.M., Li, Z., Mahlow, K., Merchant, S., Müller, J., Orsbon, C.P., Paluh, D.J., Thies, M.L., Tsai, H.P. & Witmer, L.M. (2016) Diffusible iodine-based contrast-enhanced computed tomography (diceCT): an emerging tool for rapid, high-resolution, 3-D imaging of metazoan soft tissues. *Journal of Anatomy*, 228, 889–909.
https://doi.org/10.1111/joa.12449

Goetz, A.J., Griesshaber, E., Abel, R., Fehr, T., Ruthensteiner, B. & Schmahl, W.W. (2014) Tailored order: the mesocrytalline nature of sea urchin teeth. *Acta Biomaterialia*, 10, 3885–3898.
https://doi.org/10.1016/j.actbio.2014.06.012

Grun, T.B. & Nebelsick, J.H. (2018a) Structural design of the minute clypeasteroid echinoid *Echinocyamus pusillus*. *Royal Society Open Science*, 5, 171323.
https://doi.org/10.1098/rsos.171323

Grun, T.B. & Nebelsick, J.H. (2018b) Structural design of the echinoid's trabecular system. *PLoS ONE*, 13, e0204432. https://doi.org/10.1371/journal.pone.0204432

Gusmão, L.C., Grajales, A. & Rodríguez, E. (2018) Sea anemones through X-rays: visualization of two species of *Diadumene* (Cnidaria, Actinaria) using micro-CT. *American Museum Novitates*, 3907, 1–45. https://doi.org/10.1206/3907.1

Hall, A.C., Sherlock, E. & Sykes, D. (2015) Does Micro-CT scanning damage DNA in museum specimens? *Journal of Natural Science Collections*, 2, 22–28.

Handschuh, S., Baeumler, N., Schwaha, T. & Ruthensteiner, B. (2013) A correlative approach for combining microCT, light and transmission electron microscopy in a single 3D scenario. *Frontiers in Zoology*, 10, 44. https://doi.org/10.1186/1742-9994-10-44

Handschuh, S., Beisser, C.J., Ruthensteiner, B. & Metscher, B.D. (2017) Microscopic dual-energy CT (microDECT): a flexible tool for multichannel *ex vivo* 3D imaging of biological specimens. *Journal of Microscopy*, 267, 3–26. https://doi.org/10.1111/jmi.12543

Hayward, P.J. & Ryland, J.S. (1996) *Handbook of the Marine Fauna of North-West Europe*. Oxford University Press, Oxford, 800 pp.

Hedrick, B.P., Yohe, L., Vander Linden, A., Dávalos, L.M., Sears, K., Sadier, A., Rossiter, S.J., Davies, K.T.J. & Dumont, E. (2018) Assessing soft-tissue shrinkage estimates in museum specimens imaged with diffusible iodine-based contrast-enhanced computed tomography (diceCT). *Microscopy and Microanalysis*, 24, 284–291. https://doi.org/10.1017/S1431927618000399

Herzog, H., Klein, B. & Ziegler, A. (2017) Form and function of the teleost lateral line revealed using three-dimensional imaging and computational fluid dynamics. *Journal of the Royal Society Interface*, 14, 20160898. https://doi.org/10.1098/rsif.2016.0898

Holland, N.D. & Ghiselin, M.T. (2009) Magnetic resonance imaging (MRI) has failed to distinguish between smaller gut regions and larger haemal sinuses in sea urchins (Echinodermata: Echinoidea). *BMC Biology*, 7, 39. https://doi.org/10.1186/1741-7007-7-39

Houle, D. (2010) Numbering the hairs on our heads: the shared challenge and promise of phenomics. *Proceedings of the National Academy of Sciences*, 107, 1793–1799. https://doi.org/10.1073/pnas.0906195106

Immel, A., Le Cabec, A., Bonazzi, M., Herbig, A., Temming, H., Schuenemann, V.J., Bos, K.I., Langbein, F., Harvati, K., Bridault, A., Pion, G., Julien, M.A., Krotova, O., Conard, N.J., Münzel, S.C., Drucker, D.G., Viola, B., Hublin, J.J., Tafforeau, P. & Krause, J. (2016) Effect of X-ray irradiation on ancient DNA in sub-fossil bones–guidelines for safe X-ray imaging. *Scientific Reports*, 6, 32969. https://doi.org/10.1038/srep32969

Jahn, H., Oliveira, I.D.S., Gross, V., Martin, C., Hipp, A., Mayer, G. & Hammel, J.U. (2018) Evaluation of contrasting techniques for X-ray imaging of velvet worms (Onychophora). *Journal of Microscopy*, 270, 343–358. https://doi.org/10.1111/jmi.12688

Jochum, A., Weigand, A.M., Bochud, E., Inäbnit, T., Dörge, D.D., Ruthensteiner, B., Favre, A., Martels, G. & Kampschulte, M. (2017) Three new species of *Carychium* O.F. Müller, 1773 from the Southeastern USA, Belize and Panama are described using computer tomography (CT) (Eupulmonata, Ellobioidea, Carychiidae). *ZooKeys*, 675, 97–127. https://doi.org/10.3897/zookeys.675.12453

Kato, A., Ziegler, A., Utsumi, M., Ohno, K. & Takeichi, T. (2016) Three-dimensional imaging of internal tooth structures: applications in dental education. *Journal of Oral Biosciences*, 58, 100–111. https://doi.org/10.1016/j.job.2016.05.004

Landschoff, J. & Griffiths, C.L. (2015) Three-dimensional visualisation of brooding behaviour in two distantly related brittle stars from South African waters. *African Journal of Marine Science*, 2015, 1–9. https://doi.org/10.2989/1814232X.2015.1095801

Lauer, C., Grun, T.B., Zutterkirch, I., Jemmali, R., Nebelsick, J.H. & Nickel, K.G. (2018) Morphology and porosity of the spines of the sea urchin *Heterocentrotus mamillatus* and their implications on the mechanical performance. *Zoomorphology*, 137, 139–154. https://doi.org/10.1007/s00435-017-0385-4

Lenihan, J., Kvist, S., Fernández, R., Giribet, G. & Ziegler, A. (2014) A dataset comprising four micro-computed tomography scans of freshly fixed and museum earthworm specimens. *GigaScience*, 3, 6. https://doi.org/10.1186/2047-217X-3-6

Lin, A.Y., Ding, Y., Vanselow, D.J., Katz, S.R., Yakovlev, M.A., Clark, D.P., Mandrell, D., Copper, J.E., van Rossum, D.B. & Cheng, K.C. (2018) Rigid embedding of fixed and stained, whole, millimeter-scale specimens for section-free 3D histology by micro-computed tomography. *Journal of Visualized Experiments*, 140, e58393. https://doi.org/10.3791/58293

Lucoqc, J.M., Mayhew, T.M., Schwab, Y., Steyer, A.M. & Hacker, C. (2014) Systems biology in 3D space-enter the morphome. *Trends in Cell Biology*, 25, 59–64.
https://doi.org/10.1016/j.tcb.2014.09.008

Machado, F.M., Passos, F.D. & Giribet, G. (2018) The use of micro-computed tomography as a minimally invasive tool for anatomical study of bivalves (Mollusca: Bivalvia). *Zoological Journal of the Linnean Society*, 186, 46–75.
https://doi.org/10.1093/zoolinnean/zly054

Martony, M., Pouder, D., Yanong, R., Kiryu, Y., Landsberg, J.H., Isaza, R., Waltzek, T., Stacy, N.I., Giglio, R., Baker, S. & Francis-Floyd, R. (2018) Establishing a diagnostic technique for coelomocentesis in the long-spined sea urchin *Diadema antillarum*. *Journal of Aquatic Animal Health*, 30, 325–331.
https://doi.org/10.1002/aah.10043

Masic, A. & Weaver, J.C. (2015) Large area sub-micron chemical imaging of magnesium in sea urchin teeth. *Journal of Structural Biology*, 189, 269–275.
https://doi.org/10.1016/j.jsb.2014.12.005

Metscher, B.D. (2009) MicroCT for comparative morphology: simple staining methods allow high-contrast 3D imaging of diverse non-mineralized animal tissues. *BMC Physiology*, 9, 11.
https://doi.org/10.1186/1472-6793-9-11

Metscher, B.D. (2011) X-ray microtomographic imaging of intact vertebrate embryos. *Cold Spring Harbor Protocols*, 12, 1462–1471.
https://doi.org/10.1101/pdb.prot067033

Mietchen, D., Aberhan, M., Manz, B., Hampe, O., Mohr, B., Neumann, C. & Volke, F. (2008) Three-dimensional magnetic resonance imaging of fossils across taxa. *Biogeosciences*, 5, 25–41.
https://doi.org/10.5194/bg-5-25-2008

Mihaljević, M., Jerjen, I. & Smith, A.B. (2011) The test architecture of *Clypeaster* (Echinoidea, Clypeasteroida) and its phylogenetic significance. *Zootaxa*, 2983, 21–38.
https://doi.org/10.11646/zootaxa.2983.1.2

Mihaljević, M. & Rosenblatt, A.J. (2018) A new fossil species of *Clypeaster* (Echinoidea) from Malaysian Borneo and an overview of the Central Indo-Pacific echinoid fossil record. *Swiss Journal of Paleontology*, 137, 389–404.
https://doi.org/10.1007/s13358-018-0164-y

Okanishi, M., Fujita, T., Maekawa, Y. & Sasaki, T. (2017) Non-destructive morphological observations of the fleshy brittle star, *Asteronyx loveni* using micro-computed tomography (Echinodermata, Ophiuroidea, Euryalida). *ZooKeys*, 663, 1–19.
https://doi.org/10.3897/zookeys.663.11413

Paredes, U.M., Prys-Jones, R., Adams, M., Groombridge, J., Kundu, S., Agapow, P.M. & Abel, R.L. (2012) Micro-CT X-rays do not fragment DNA in preserved bird skins. *Journal of Zoological Systematics and Evolutionary Research*, 50, 247–250.
https://doi.org/10.1111/j.1439-0469.2012.00657.x

Rahman, I.A. & Clausen, S. (2009) Re-evaluating the palaeobiology and affinities of the Ctenocystoidea (Echinodermata). *Journal of Systematic Palaeontology*, 7, 413–426.
https://doi.org/10.1017/S1477201909990046

Rahman, I.A. & Zamora, S. (2009) The oldest cinctan carpoid (stem-group Echinodermata) and the evolution of the water vascular system. *Zoological Journal of the Linnean Society*, 157, 420–432.
https://doi.org/10.1111/j.1096-3642.2008.00517.x

Rahman, I.A., Belaústegui, Z., Zamora, S., Nebelsick, J.H., Domènech, R. & Martinell, J. (2015) Miocene *Clypeaster* from Valencia (E Spain): insights into the taphonomy and ichnology of bioeroded echinoids using X-ray micro-tomography. *Palaeogeography, Palaeoclimatology, Palaeoecology*, 438, 168–179.
https://doi.org/10.1016/j.palaeo.2015.07.021

Reich, M. (2015) Different pathways in early evolution of the holothurian calcareous ring? *Cuadernos del Museo Geominero*, 19, 137–145.

Reid, M., Bordy, E.M., Taylor, W.L., le Roux, S.G. & du Plessis, A. (2018) A micro X-ray computed tomography dataset of fossil echinoderms in an ancient obrution bed: a robust method for taphonomic and palaeoecologic analyses. *GigaScience*, 8, 1–8.
https://doi.org/10.1093/gigascience/giy156

Rowe, T. & Frank, L.R. (2011) The disappearing third dimension. *Science*, 331, 712–714.
https://doi.org/10.1126/science.1202828

Sadler, T., Kroh, A. & Gallagher, S.J. (2016) A review of the taxonomy and systematics of the echinoid genus *Monostychia* Laube, 1869. *Alcheringia*, 40, 341–353.
https://doi.org/10.1080/03115518.2016.1144362

Schindelin, J., Arganda-Carreras, I., Frise, E., Kaynig, V., Longair, M., Pietzsch, T., Preibisch, S., Rueden, C., Saalfeld, S., Schmid, B., Tinevez, J.Y., White, D.J., Hartenstein, V., Eliceiri, K., Tomancak, P. & Cardona, A. (2012) Fiji: an open-source platform for biological-image analysis. *Nature Methods*, 9, 676–682.
https://doi.org/10.1038/nmeth.2019

Schmidbaur, J., Keklikoglou, L., Metscher, B.D. & Faulwetter, S. (2015) Exploring methods to remove iodine and phosphotungstic acid from zoological specimens. *In*: *Micro-CT 2015 User Meeting Abstract Book*, Brugge, pp. 109–116.

Schwertmann, L., Focke, O. & Dirks J.-H. (2019) Morphology, shape variation and movement of skeletal elements in starfish (*Asterias rubens*). *Journal of Anatomy*, 234, 656–667.
https://doi.org/10.1111/joa.12964

Sigl, R., Imhof, H., Settles, M. & Laforsch, C. (2013) A novel, non-invasive and *in vivo* approach to determine morphometric data in starfish. *Journal of Experimental Marine Biology and Ecology*, 449, 1–9.
https://doi.org/10.1016/j.jembe.2013.08.002

Sombke, A., Lipke, E., Michalik, P., Uhl, G. & Harzsch, S. (2015) Potential and limitations of X-ray micro-computed tomography in arthropod neuroanatomy: a methodological and comparative survey. *The Journal of Comparative Neurology*, 523, 1281–1295.
https://doi.org/10.1002/cne.23741

Souto, C. & Martins, L. (2018) Synchrotron micro-CT scanning leads to the discovery of a new genus of morphologically conserved echinoid (Echinodermata: Cassiduloida). *Zootaxa*, 4457 (1), 70–92.
https://doi.org/10.11646/zootaxa.4457.1.3

Stauber, M. & Müller, R. (2008) Micro-computed tomography: a method for the non-destructive evaluation of the three-dimensional structure of biological specimens. *Methods in Molecular Biology*, 455, 273–292.
https://doi.org/10.1007/978-1-59745-104-8_19

Stock, S.R., Barss, J., Dahl, T., Veis, A. & Almer, J.D. (2002) X-ray absorption microtomography (microCT) and small beam diffraction mapping of sea urchin teeth. *Journal of Structural Biology*, 139, 1–12.
https://doi.org/10.1016/S1047-8477(02)00500-2

Stock, S.R., De Carlo, F., Xiao, X. & Ebert, T.A. (2010) Bridges between radial wedges (septs) in two diadematid spine types. *In*: Harris, L.G., Böttger, S.A., Walker, C.W. & Lesser, M.P. (Eds.), *Echinoderms: Durham. Proceedings of the 12th International Echinoderm Conference, Durham, New Hampshire, USA, 7-11 August 2006*. A.A. Balkema, Leiden/London/New York/Philadelphia/Singapore, pp. 263–267.
https://doi.org/10.1201/9780203869543-c43

Stock, S.R., Ebert, T.A., Ignatiev, K. & De Carlo, F. (2006) Structures, structural hierarchy and function in sea urchins spines. *Proceedings of SPIE*, 6318, 63180A.
https://doi.org/10.1117/12.679548

Stock, S.R., Ignatiev, K. & De Carlo, F. (2004b) Very high resolution synchrotron microCT of sea urchin ossicles. *In*: Heinzeller, T. & Nebelsick, J.H. (Eds.), *Echinoderms: München-Proceedings of the 11th International Echinoderm Conference*, *6-10 October 2003, Munich, Germany*. CRC Press, London, pp. 353–358.
https://doi.org/10.1201/9780203970881.ch58

Stock, S.R., Ignatiev, K.I., Veis, A., De Carlo, F. & Almer, J.D. (2004a) MicroCT of sea urchin ossicles supplemented with microbeam diffraction. *Proceedings of SPIE*, 5535, 11–20.
https://doi.org/10.1117/12.558070

Stock, S.R., Nagaraja, S., Barss, J., Dahl, T. & Veis, A. (2003) X-ray microCT study of pyramids of the sea urchin *Lytechinus variegatus*. *Journal of Structural Biology*, 141, 9–21.
https://doi.org/10.1016/S1047-8477(02)00554-3

Stock, S.R. & Rack, A. (2014) Submicrometer structure of sea urchin tooth via remote synchrotron microCT imaging. *Proceedings of SPIE*, 9212, 92120V.
https://doi.org/10.1117/12.2062976

Stock, S.R., Seto, J., Deymier, A.C., Rack, A. & Veis, A. (2017) Growth of second stage mineral in *Lytechinus variegatus*. *Connective Tissue Research*, 59, 345–355.
https://doi.org/10.1080/03008207.2017.1391233

Stock, S.R., Veis, A., Ciao, X., Almer, J.D. & Dorvee, J.R. (2012) Sea urchin tooth mineralization: calcite present early in the aboral plumula. *Journal of Structural Biology*, 180, 280–289.
https://doi.org/10.1016/j.jsb.2012.08.004

Stock, S.R., Xiao, X., Stock, S.R. & Ziegler, A. (2013) Quantification of carinar process plate orientation in camarodont sea urchin teeth. *Cahiers de Biologie Marine*, 54, 735–741.

Tessler, M., Barrio, A., Borda, E., Rood-Goldman, R., Hill, M. & Siddall, M.E. (2016) Description of a soft-bodied invertebrate with microcomputed tomography and revision of the genus *Chtonobdella* (Hirudinea: Haemadipsidae). *Zoologica Scripta*, 45, 552–565.
https://doi.org/10.1111/zsc.12165

Wanek, J. & Rühli, F.J. (2016) Risk to fragmented DNA in dry, wet, and frozen states from computed tomography: a comparative theoretical study. *Radiation and Environmental Biophysics*, 55, 229–241. https://doi.org/10.1007/s00411-016-0637-6

Weinhardt, V., Shkarin, R., Wernet, T., Wittbrodt, J., Baumbach, T. & Loosli, F. (2018) Quantitative morphometric analysis of adult teleost fish by X-ray computed tomography. *Scientific Reports*, 8, 16531. https://doi.org/10.1038/s41598-018-34848-z

Xavier, J.C., Allcock, A.L., Cherel, Y., Lipinski, M.R., Pierce, G.J., Rodhouse, P.G.K., Rosa, R., Shea, E.K., Strugnell, J.M., Vidal, E.A.G., Villanueva, R. & Ziegler, A. (2015) Future challenges in cephalopod research. *Journal of the Marine Biological Association of the United Kingdom*, 95, 999–1015. https://doi.org/10.1017/S0025315414000782

Zamora, S., Rahman, I.A. & Smith, A.B. (2012) Plated Cambrian bilaterians reveal the earliest stages of echinoderm evolution. *PLoS ONE*, 7, e38296. https://doi.org/10.1371/journal.pone.0038296

Zanette, I., Daghfous, G., Weitkamp, T., Gillet, B., Adriaens, D., Langer, M., Cloetens, P., Helfen, L., Bravin, A., Peyrin, F., Baukbach, T., Dischler, J.M., Van Loo, D., Praet, T., Poirier-Quinot, M. & Boistel, R. (2014) Looking inside marine organisms with magnetic resonance and X-ray imaging. *In*: Reynaud, E.G. (Ed.), *Imaging Marine Life: Macrophotography and Microscopy Approaches for Marine Biology*. Wiley-VCH, Weinheim, pp. 123–184. https://doi.org/10.1002/9783527675418.ch7

Zehbe, R., Haibel, A., Riesemeier, H., Gross, U., Kirkpatrick, C.J., Schubert, H. & Brochhausen, C. (2010) Going beyond histology-synchrotron micro-computed tomography as a methodology for biological tissue characterization: from tissue morphology to individual cells. *Journal of the Royal Society Interface*, 7, 49–59. https://doi.org/10.1098/rsif.2008.0539

Zehbe, R., Riesemeier, H., Kirkpatrick, C.J. & Brochhausen, C. (2012) Imaging of articular cartilage-data matching using X-ray tomography, SEM, FIB slicing and conventional histology. *Micron*, 43, 1060–1067. https://doi.org/10.1016/j.micron.2012.05.001

Ziegler, A. (2012) Broad application of non-invasive imaging techniques to echinoids and other echinoderm taxa. *Zoosymposia*, 7, 53–70. https://doi.org/10.11646/zoosymposia.7.1.6

Ziegler, A. (2014) Rediscovery of an internal organ in heart urchins (Echinoidea: Spatangoida): morphology and evolution of the intestinal caecum. *Organisms Diversity & Evolution*, 14, 383–395. https://doi.org/10.1007/s13127-014-0178-2

Ziegler, A. (2019) Combined visualization of echinoderm hard and soft parts using contrast-enhanced micro-computed tomography. Morphobank, Project #3268. [https://morphobank.org/index.php/Projects/ProjectOverview/project_id/3268]

Ziegler, A. & Angenstein, F. (2007) Analyse von Seeigeln mit Hilfe der bildgebenden Magnetresonanztomographie. *Mikrokosmos*, 96, 49–54.

Ziegler, A. & Barr, D.J. (2018) The historical and biographical context of Gregory's diverticulum, an unusual organ in sand dollars. *Breviora*, 559, 1–18. https://doi.org/10.3099/MCZ47.1

Ziegler, A. & Bartolomaeus, T. (2009) Magnetic resonance imaging: a powerful tool in comparative morphology despite initial interpretative difficulties. *In*: Holland, N.D. & Ghiselin, M.T., *Magnetic resonance imaging (MRI) has failed to distinguish between smaller gut regions and larger haemal sinuses in sea urchins (Echinodermata: Echinoidea)*. *BMC Biology*, 7, 39, 2–3. https://doi.org/10.1186/1741-7007-7-39

Ziegler, A., Bartolomaeus, T. & Mueller, S. (2010c) Sea urchin (Echinoidea) anatomy revealed by magnetic resonance imaging and 3D visualization. *In*: Harris, L.G., Böttger, S.A., Walker, C.W. & Lesser, M.P. (Eds.), *Echinoderms: Durham. Proceedings of the 12th International Echinoderm Conference, Durham, New Hampshire, USA, 7-11 August 2006*. A.A. Balkema, Leiden/London/New York/Philadelphia/Singapore, pp. 305–310. https://doi.org/10.1201/9780203869543-c50

Ziegler, A., Bock, C., Ketten, D.R., Mair, R.W., Mueller, S., Nagelmann, N., Pracht, E.D. & Schröder, L. (2018) Digital three-dimensional imaging techniques provide new analytical pathways for malacological research. *American Malacological Bulletin*, 36, 248–273. https://doi.org/10.4003/006.036.0205

Ziegler, A., Faber, C. & Bartolomaeus, T. (2009) Comparative morphology of the axial complex and interdependence of internal organ systems in sea urchins (Echinodermata: Echinoidea). *Frontiers in Zoology*, 6, 10. https://doi.org/10.1186/1742-9994-6-10

Ziegler, A., Faber, C., Mueller, S. & Bartolomaeus, T. (2007) High-field MR microscopy as a tool for comparative morphological studies: soft tissue discrimination in sea urchins. *Proceedings of the International Society for Magnetic Resonance in Medicine*, 15, 1340.

Ziegler, A., Faber, C., Mueller, S. & Bartolomaeus, T. (2008) Systematic comparison and reconstruction of sea urchin (Echinoidea) internal anatomy: a novel approach using magnetic resonance imaging. *BMC Biology*, 6, 33. https://doi.org/10.1186/1741-7007-6-33

Ziegler, A., Faber, C., Mueller, S., Nagelmann, N. & Schröder, L. (2014) A dataset comprising 141 magnetic resonance imaging scans of 98 extant sea urchin species. *GigaScience*, 3, 21. https://doi.org/10.1186/2047-217X-3-21

Ziegler, A., Kunth, M., Mueller, S., Bock, C., Pohmann, R., Schröder, L., Faber, C. & Giribet, G. (2011a) Application of magnetic resonance imaging in zoology. *Zoomorphology*, 130, 227–254. https://doi.org/10.1007/s00435-011-0138-8

Ziegler, A., Lenihan, J., Zachos, L.G., Faber, C. & Mooi, R. (2016) Comparative morphology and phylogenetic significance of Gregory's diverticulum in sand dollars (Echinoidea: Clypeasteroida). *Organisms Diversity & Evolution*, 16, 141–166. https://doi.org/10.1007/s13127-015-0231-9

Ziegler, A. & Menze, B.H. (2013) Accelerated acquisition, visualization, and analysis of zoo-anatomical data. *In*: Zander, J. & Mostermann, P.J. (Eds.), *Computation for Humanity: Information Technology to Advance Society*. CRC Press, Boca Raton, pp. 233–261.

Ziegler, A., Mietchen, D., Faber, C., von Hausen, W., Schöbel, C., Sellerer, M. & Ziegler, A. (2011b) Effectively incorporating selected multimedia content into medical publications. *BMC Medicine*, 9, 17. https://doi.org/10.1186/1741-7015-9-17

Ziegler, A., Mooi, R., Rolet, G. & De Ridder, C. (2010d) Origin and evolutionary plasticity of the gastric caecum in sea urchins (Echinodermata: Echinoidea). *BMC Evolutionary Biology*, 10, 313. https://doi.org/10.1186/1471-2148-10-313

Ziegler, A. & Mueller, S. (2011) Analysis of freshly fixed and museum invertebrate specimens using high-resolution, high-throughput MRI. *Methods in Molecular Biology*, 771, 633–651. https://doi.org/10.1007/978-1-61779-219-9_32

Ziegler, A., Ogurreck, M. & Beckmann, F. (2010b) Large-scale comparative morphological studies of sea urchins (Echinodermata: Echinoidea) using µCT and SRµCT. *DESY Annual Report Photon Science, Hamburg.* Available from: http://photon-science.desy.de/annual_report/files/2010/20101262.pdf (accessed 4 September 2019)

Ziegler, A., Ogurreck, M., Steinke, T., Beckmann, F., Prohaska, S. & Ziegler, A. (2010a) Opportunities and challenges for digital morphology. *Biology Direct*, 5, 45. https://doi.org/10.1186/1745-6150-5-45

Ziegler, A., Schröder, L., Ogurreck, M., Faber, C. & Stach, T. (2012b) Evolution of a novel muscle design in sea urchins (Echinodermata: Echinoidea). *PLoS ONE*, 7, e37520. https://doi.org/10.1371/journal.pone.0037520

Ziegler, A., Stock, S.R., Menze, B.H. & Smith, A.B. (2012a) Macro-and microstructural diversity of sea urchin teeth revealed by large-scale micro-computed tomography survey. *Proceedings of SPIE*, 8506, 85061G. https://doi.org/10.1117/12.930832